

Article

Influence of Symmetry of Tightened Parts on the Force in a Bolted Joint

Jiri Zacal , Zdenek Folta, Jiri Struz  and Miroslav Trochta 

Department of Machine Parts and Mechanisms, Faculty of Mechanical Engineering, VSB-Technical University of Ostrava, 70800 Ostrava-Poruba, Czech Republic

* Correspondence: jiri.zacal@vsb.cz; Tel.: +420-596-993-288

Abstract: This article discusses the issue of force behavior in a pre-tensioned bolt that is part of a symmetrical flange connection, loaded with an operating load parallel to the bolt axis. The first part describes the issue being dealt with in detail. The next part offers a brief description of the generally known theoretical approach to the solution, and also outlines the limitations of this approach. This part is followed by a theoretical analysis of working load behavior in the bolt of the analyzed device, using Finite Element Method (FEM). In this article, a comparison of several different approaches to the solution can be also found, followed by a description of the experiment preparation and its results. The obtained values also serve as a subject for reverse iterative analysis carried out using ANSYS software. The aim is to find a proper modification to the symmetric calculation model that would be consistent with the results of measurements from technical practice. All results achieved are described in the final part of the article.

Keywords: bolt; screw; flange; operating load; bolt pre-tension; bolt working load; bolted joint; strain gauge; bolted joint diagram; preload; stiffness; flatness of contact surfaces

1. Introduction

Bolted connections are among the most used machine components and are practically irreplaceable in technical practice. It might seem that nowadays this issue is already clarified, but the opposite is true. It is the commonness and experience of this component that leads many to the opinion that the bolt is a simple machine component that can also be easily calculated in terms of strength. In engineering practice, rather primitive calculations are sometimes used. Often a simple bolted joint diagram is used, but no attention is given to the correct definition of the components stiffness. It is necessary to define exactly which parts of the bolted connection are further compressed by the operating force and which are, on the opposite, relieved. It is also very important to define the position of the operating force in relation to the contact surface of the flanges and the bolt axis. In terms of stress distribution, the bolt itself is a very complex component. The situation becomes even more difficult if it is a multi-bolted joint with complicated (asymmetrical) flange shapes or complex operating force applications in critical ambient conditions (e.g., intercoolers in nuclear power plants, pressure vessels in the petrochemical and chemical industries, automotive components, etc.). Pre-tensioned bolted joints are often critically stressed and are often part of critical equipment. The progress of these devices has not stopped nowadays, and for this reason it is very important to continue research in the field of bolts, which are an integral part of them.

The issue dealt with in this article arose based on requirements made by the rolling mill operator. The aim was to determine the rolling forces generated during the passage of rolled products through the rollers. The initial solution was to propose a suitable methodology for measuring this load without the need for any significant modification of the existing mill structure. Two measurement methods were considered, namely installing a commercial force sensor or installing strain gauges on a suitable part of the structure.



Citation: Zacal, J.; Folta, Z.; Struz, J.; Trochta, M. Influence of Symmetry of Tightened Parts on the Force in a Bolted Joint. *Symmetry* **2023**, *15*, 276. <https://doi.org/10.3390/sym15020276>

Academic Editor: Raffaele Barretta

Received: 7 December 2022

Revised: 11 January 2023

Accepted: 17 January 2023

Published: 19 January 2023



Copyright: © 2023 by the authors. Licensee MDPI, Basel, Switzerland. This article is an open access article distributed under the terms and conditions of the Creative Commons Attribution (CC BY) license (<https://creativecommons.org/licenses/by/4.0/>).

For this rolling mill, the model of which is displayed in Figure 1, the pressure force of the rollers is generated by the central bolt and nut in bearing location. All connected parts of the rolling mill were made of S355J2G3 steel.

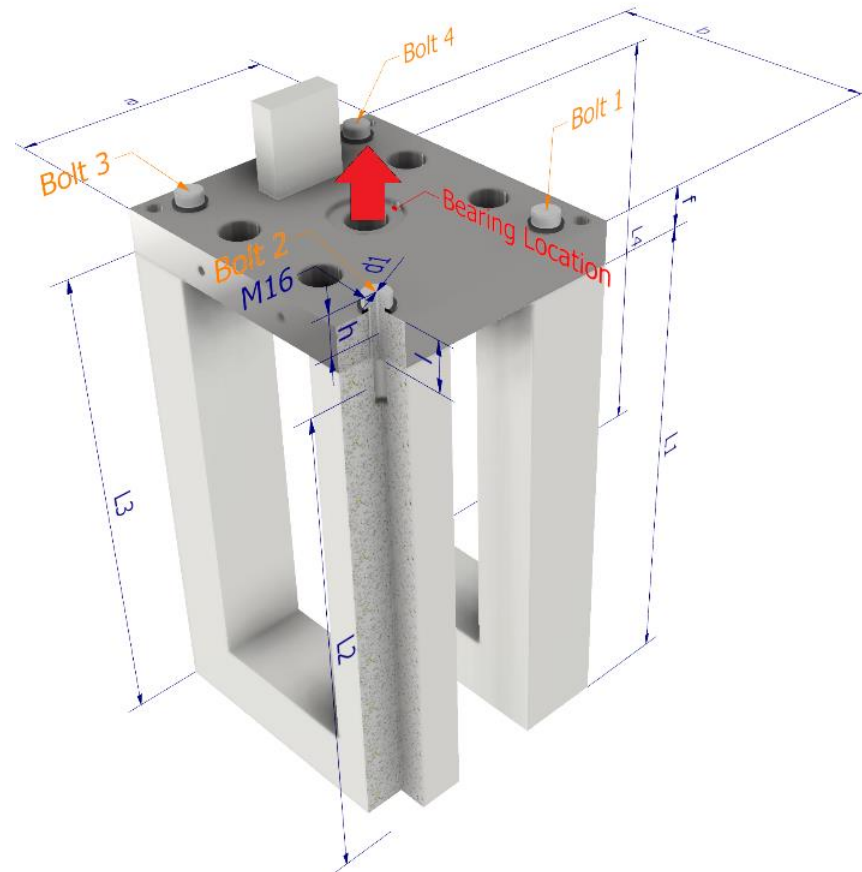


Figure 1. Dimension schematic diagram of the rolling mill.

In the area of this bolt placement, no suitable space was found either for the installation of the sensor, if the bearing plate was not reconstructed, or for the strain gauges. Another suitable place to mount strain gauges was on the four legs of the frame. However, this option was rejected due to relatively little expected stress values and thus the small values of the signal from the strain gauges. Another reason was the installation of a number of holders for other technological equipment and covers that, as result, changed the stiffness of these legs and brought considerable uncertainty to the resulting value of the measured forces. Finally, four M16 bolts with property class 8.8 were used for measurements, which symmetrically attached the top plate to the legs of the frame.

As part of the research into the current state of the field of bolted joints, the first phase of the literature search focused on various methods of measuring bolt preload other than the use of strain gauges, such as using ultrasound, piezoelectric sensors, special impact testing of a bolt head [1] or using automatic digital image correlation [2]. However, it is necessary to consider the fact that the measurement will take place during operation (i.e., there is influence of dynamic impacts, noise, vibrations). Furthermore, the aim would be to achieve low production costs.

As part of the research of the current state of the field of bolted joints, the literature focusing on various alternative measurement methods, such as in [1,2], was investigated in the first phase. In the following, the study of literature sources focused on existing theoretical calculation procedures, which are presented, e.g., in [3] and [4]. Attention was also given to new methods of calculations as reported by Y. Tian [5]. Previous research on the effect of the asymmetry of a multi-bolted connection on the asymmetry of the connected

pressure vessel shell has also provided an important basis for solving the problem, see [6]. A key source of information is the book by F. Pospisil [7], which is still one of the most detailed summaries of knowledge about bolted connections based on experiments and practical experience. Numerical calculation methods (FEM), as an alternative to existing theoretical approaches, have also been studied further in [8–10]. It has also proved very appropriate to combine the numerical approach with the experimental one as did T. Benhaddou [11]. For the simplified FE computational model, the information in [12] was helpful. The FEM calculations verified the nature of the stress flow with the already known assumptions given in the literature [13,14]. This step served mainly as a verification of the correctness of the computational model. An important section in the development of the computational model was also its simplification. For this purpose, the information presented in [15–17], which describes the load and stress behavior across the contact threaded region of the bolt, was very useful. Other references were crucial in terms of the design and execution of the experiment, e.g., basic information [18] or advanced information from N. Fric [19] about the limitations of strain gauging when using internal strain gauges in bolts. Publications [20–22] dealing with the issue of bolt tightening accuracy (achieving bolt preload) were also examined. This information serves mainly to show the scope of the bolted connections issue. Furthermore, this knowledge was used to design the first phase of the experiment, which was precisely the verification of the achieved bolt pre-tension. Since bolted connections have a wide range of applications, it was easy to get into areas that are far from the topic of the article at first view. As an example, in reference [23], they dealt with the problem of a bolt fasten wedge active joint for braced excavations. However, it is in this paper that one can see the asymmetric behavior of loads with relation to bolts for apparently symmetric components. The limitation of the measurements by a single strain gauge placed on the outer shell of the bolt shank is also well seen. Additionally, there have been publications by P. Sharos [24] and V. Belardi [25]. In one paper [24], a finite-element model capable of modeling bolted joints under different loading rates was proposed. The design was made for an epoxy composite material joint with carbon fibers. The bolt material was defined as titanium alloy. Furthermore, a shear quasi-static load of up to 10 m/s perpendicular to the bolt axis was applied. The elements of the computational model were designed as shells. However, the problem solved in this paper differs not only in the material (all elements are steel) but also in the loading, which is time independent and, in a direction, parallel to the bolt axis. In addition, the ANSYS software, which is used here, has a custom object used to efficiently solve bolted connections. Another approach to solving composite bolted joints using FE modelling, which are loaded by a force perpendicular to the bolt axis, is presented in [25]. However, here the relationship between the bolt and the plates has been modelled as a beam on an elastic base.

The main aim of this article is to examine the issue of symmetry deviations of clamped parts (see Figure 1) in the calculation of pre-tensioned bolt joints loaded with an operating load parallel to the bolt axis. Preloaded bolted joints are usually highly stressed machine components. Thus, even seemingly small effects of the asymmetry of the clamped assembly can have a significant effect on the reliability and safety of the component. Using experiments and FEM, some influence of asymmetry has been demonstrated. This knowledge can be particularly useful for applications where critically loaded bolted joints are involved. The results obtained have been described in more detail in the conclusion.

2. Description of the Basic Approach to Solving Bolted Joints

The use of bolts to provide measurements of the operating force, in this case, offers a number of advantages, such as sufficiently large measured stresses, the possibility to prepare measuring bolts in laboratory conditions, and the control of the real achieved pre-tension. Nevertheless, it is also related to the need for an analytical recalculation of the measured values, which can introduce some inaccuracies into the measurement.

Theoretical recalculation is commonly used and seems to be a very simple method. The basic procedure is given, for example, in [3] or in [4]. The basic principle is that the

operating load F acting on the tightened bolt (see Figure 2) is not reflected in its entirety in the bolt load F_S , but only a part of it (another part is also reflected in the clamping of the flanges F_F). The size of this part depends on the stiffness of both the bolt and the compressed parts (hereinafter referred to as the “flange”). Stiffness is defined here as the ratio of force F to the current deformation, i.e., the compression of the flange or stretching of the bolt by Δl .

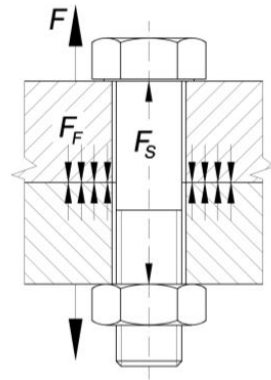


Figure 2. Forces acting in bolted joint.

The basic principle of the simplified theoretical calculation can also be clearly seen in the bolted connection diagram (see Figure 3), which is used to depict the force and deformation relationships in a prestressed bolted connection. The bolted joint diagram is in principle based on the stress–strain curve of the material, but only for the linear region (up to the proportional limit). In the elastic limit region, both the stiffness angle α and the modulus of elasticity E are constant. The final form of the diagram was obtained by combining the stiffness lines of the tension-loaded components (a -line for bolt) with the stiffness line for the compression-loaded components (b -line for flanges) so that the sum of their deformations ($\Delta l_S, \Delta l_F$) is the deformation of the whole system Δl . For this purpose, the stiffness line of the compressed parts is moved to point C where the prestressing effect F_B is the same, only with the opposite load polarity (see Figure 3). Then, ΔF_S is the force increase in the bolt and ΔF_{FF} is the clamping force decrease in the contact between the flanges. The force F represents the operating tensile load. The F_S is the total force in the bolt during operation. The parameter F_F is the residual clamping force in the flange contact, which also characterizes the tightness of the joint. In the case of the example shown in Figure 3, it is possible in principle to calculate the stiffness of bolt C_S and flange C_F using the following general relations:

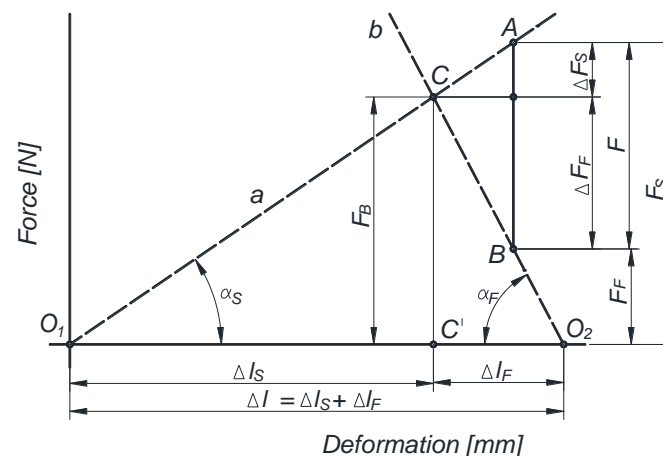


Figure 3. The Basic Bolted Joint Diagram.

$$C_S = tg \alpha_S = \frac{F}{\Delta l_S} = \frac{E_S \cdot S_S}{l} \quad (1)$$

$$C_F = tg \alpha_F = \frac{F}{\Delta l_F} = \frac{E_F \cdot S_F}{l} \quad (2)$$

where:

C_S Bolt stiffness

C_F Flange stiffness

E Modulus of elasticity defined by a low index

S Load bearing (deformable) cross-section defined by a low index

α Angle of inclination for stiffness line, defined by a low index

The low index "S" is the designation for the bolt and low index "F" is for the flange.

In the case of Force [N], a variable cross section along the length of the bolt, the total elongation or shortening λ is calculated as:

$$\lambda = \frac{F_B}{E_S} \int_0^l \frac{1}{S_x} dx = F_v \cdot \frac{Y}{E} \quad (3)$$

F_B Pre-tensioning of the bolt

E_S Modulus of elasticity of the bolt

l Analyzed axial length

S_x Elementary axial surface of the shape

Y The entire surface of the shape

For a bolt with a simple shape, the calculation can be simplified by dividing the bolt into sections of the same cross section. The resulting stiffness of the entire bolt is then determined from the sum of the elastic compliances of the partial sections according to the relationship:

$$\frac{1}{C_S} = \frac{1}{E_S} \left(\sum \frac{l_i}{S_i} \right) \quad (4)$$

where:

C_S Bolt stiffness

E_S Modulus of elasticity of the bolt

l_i Partial lengths of the bolt parts

S_i Relevant load-bearing cross-sections

The bolt head in this case is calculated as an extension of the diameter under the head up to 2/3 of the head height, in the case of a thread as an extension of the threaded part by 1/2 of the matrix height (see Figure 4).

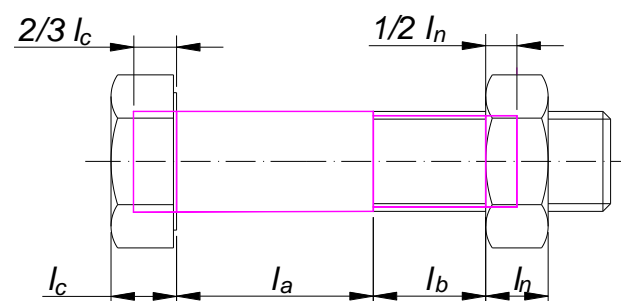


Figure 4. Bolt dimension schema.

In the case of flanges, the determination of stiffness is a bit more complex, as only a part of the flange in close proximity to the bolt-bearing surface is involved in the deformation due to pre-tensioning. Most often, the deformed area is approximately bounded by the so-called Bach's double cone (frustum double cone) joint with the angle of inclination of

45° for steels. It should be stated that in reality, the size of this angle (see Figure 5) can differ. Moreover, this angle is very important from a technical point of view and also serves as a basis for new calculation methodologies, e.g., see [5]. However, this issue will be described in more detail in Section 3. For the calculation, this double cone can be simply replaced by a Rötischer cylinder (dashed line in Figure 5) with an internal diameter corresponding to the drilled hole D_o and outer dimension D_R .

$$D_R = s + \frac{l}{2} \cdot \operatorname{tg} \alpha \quad (5)$$

where:

D_R Outer dimension of Rötischer cylinder

s Outer diameter of bearing surface (Width across flats)

α Angle of frustum double cone

The area of the Rötischer frustum cone envelope is then:

$$S_R \cong \frac{\pi}{4} \left[\left(s + \frac{l}{2} \cdot \operatorname{tg} \alpha \right)^2 - D_o^2 \right] \quad (6)$$

where:

D_o Diameter of drilled hole

l Clamped length

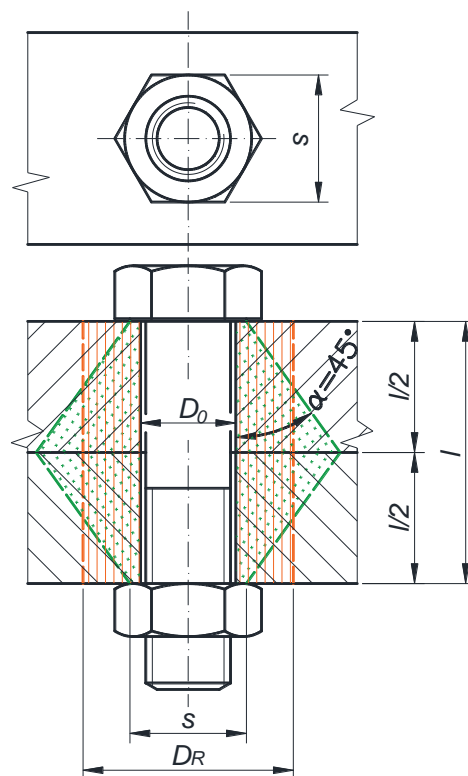


Figure 5. Theoretical determination of the deformed area of the flange.

It is therefore a simplified calculation for the cases where it is not possible to determine the stiffness of the flanges in any other way. More accurate values can be obtained either by experiment or using Finite Element Method (FEM) analysis. Complications arise if the bolt joint is not equipped with a nut and is tightened into a threaded hole (Figure 6), which was the case that was being sold.

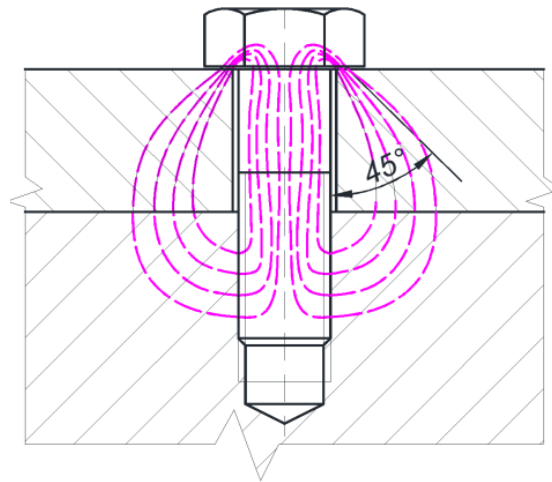


Figure 6. Approximate lines of force for the bolt in the threaded hole.

The distribution of stress is more complex and its replacement using Bach's double cone joint is then rather speculative. Only a one-sided cone in the direction of the drilled bolt head is considered (see Figure 7).

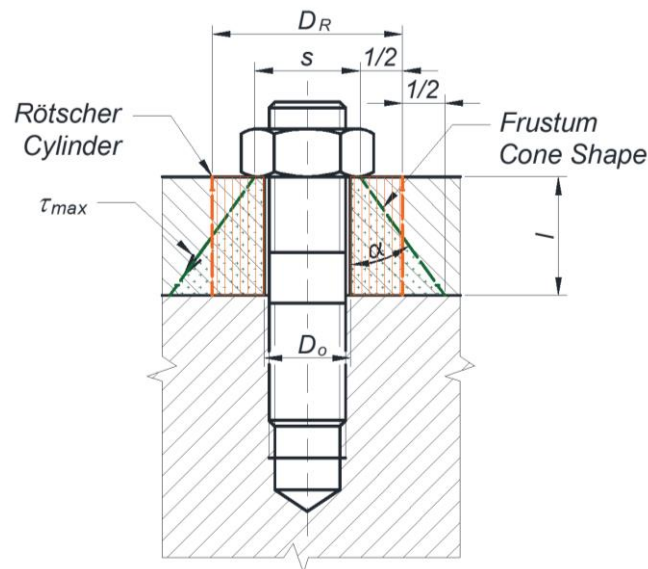


Figure 7. Theoretical determination of the deformed area in the stud bolt.

Then the relationship applies:

$$S_{R1} \cong \frac{\pi}{4} \left[(s + l \cdot \tan \alpha)^2 - D_0^2 \right] \quad (7)$$

Note. All symbols in Equation (7) correspond to the description in Equation (6).

However, there is another issue. The size of the force increase in the bolt ΔF_S (see Figure 3) from the operational force is not dependent only on the stiffnesses C_S and C_F . Previous research in the field of flanges (especially circular) joints has shown that the behavior of the load force in the bolt is also influenced by the position of the point of the operational force, see [7] (p. 161) and [6]. This location may be subject to change during operation, especially in the case of joints where significant deformations occur due to the operating load (e.g., the flange joints of thin-walled vessels). Even more complicated is the situation when using a gasket that can change its stiffness nonlinearly (according to the material used) depending on the load, allowing for even greater deformation. In addition, the gasket is permanently deformed. In the area of the circular joints of pressure vessels, it

turned out that the asymmetry of the connected envelope also has a significant influence on the magnitude of the operating force in the bolt. A detailed description of this issue is given in [6].

The diagram of the pre-tensioned bolt connection shown in Figure 3 assumes an unchanged stiffness between the mounting and operating states. It also assumes that the bolt is lengthened (loaded) by the operating force, while the flanges are only lightened. Operating loads directly affect the bearing surface of the bolt head and its nut. This is a very simplified case that rarely occurs in practice. In reality, the assembly and operation diagrams may differ (usually such diagrams are displayed together). This difference can be due, for example, to a change in ambient temperature, or the already mentioned change in the point of application of the operating force in relation to the mounting pre-tensioning. Thus, there can be also a change in the parts that are further loaded due to the operating load and the parts that in turn are lightened. Defining the stiffness of loaded or lightened parts is not easy, and, in some cases, is not even theoretically possible [7] (p. 164). This also prevents an accurate recalculation of the force increment parameter in the bolt ΔF_S , which in our case is necessary for the calculation of the resulting rolling force F (see Figure 8). The above-mentioned aspects greatly influenced the following steps of the experiment preparation.

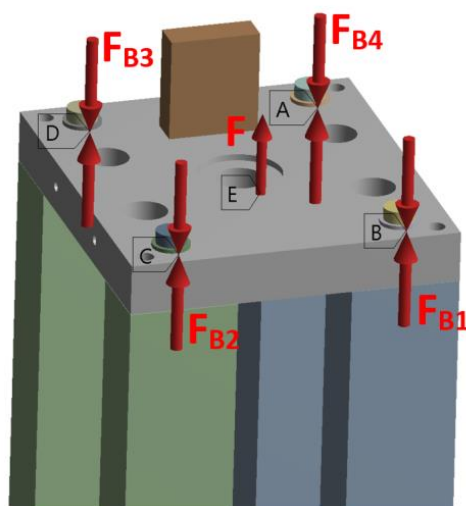


Figure 8. Load specification in finite element solid model.

3. Finite Element Analysis of Force Behavior in the Bolt

As mentioned earlier, the special design of the rolling mill did not allow us to make an experimental determination directly to find the magnitude of the operating rolling force. It was necessary to measure the influence of this force on partial increases in forces acting in the bolt and then recalculate them. As a result of certain concerns about the behavior of the force in the bolt that is in operation, mentioned in Section 2, it was decided that the recalculation would not be carried out based on the theory mentioned in Section 2, but FE analysis using ANSYS software will be carried out.

This method of solution is typical for similar more complex cases of loading of multi-bolt connections, either for assembly or operating conditions [8,9]. An example of how the finite element method can be useful in improving or replacing existing calculation methods of a bolted connection of an end-plate cantilever beam can be found, for example, in [10]. Especially if it is combined with measurement in real conditions, i.e., with an experiment, the numerical approach has also proven successful in solving the effect of axial preload on the fatigue life of fastened joints in the aerospace industry [11]. Thus, in the first phase, a calculation model was created (see Figure 8).

Ideal geometry of Solid type was used for modelling, without considering the clearances in contacts, production inaccuracies, bolt threads, etc. The threaded part of the bolt

was replaced by a cylinder with a diameter of 13.546 mm, which corresponds to the minor diameter of M16 bolt size. Contacts were set up as Frictional support with a coefficient of friction of 0.1. A shear friction coefficient of 0.2 was set between the contact surfaces of the leg and the pressure plates. To connect bolts with the individual legs, a binding Bonded was used. The base of the legs for the rolling mill was anchored using a Fixed Support. Pre-tensioning in the bolts was carried out using the object Bolt Pre-tension, which splits a bolt into two parts joined by a constraint of equations to define the tension behavior. Pre-tensioning of the bolt F_B for assembly status was always set to 60,000 N. The bolt preload value was determined on the basis of the prescribed tightening torque specified in the operating documentation of the equipment.

Figure 9 shows the mesh character used in the computational model. A higher order 3D 20-node solid element that exhibits quadratic displacement behavior was used to create the mesh, or possibly a high-order 3D, 10-node element if there was no other option. The maximum element size for the legs and flange was set to 8 mm, for the bolts and washers the maximum element size was set to 2 mm. The analysis of mesh convergence was performed by varying the size of the mesh until it was proven that the size of the elements had no significant effect on the results. It should be taken into account that in this case the primary result is not the stress flow, but the value of the change in the working force in the bolt. It is assumed that in this case the effect of mesh size is not as impactful with regard to the results. Figure 9a depicts the mesh character of the computational model of the coupling assembly. Figure 9b then shows the mesh on the bolt shank.

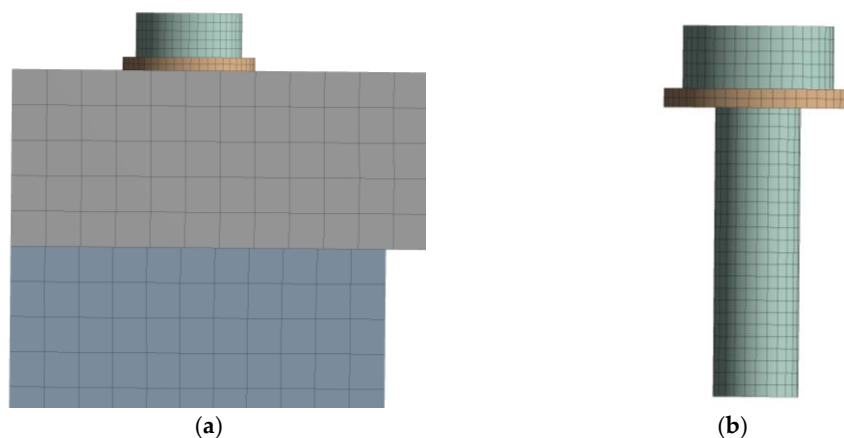


Figure 9. Specification of the computational model mesh.

The material properties of the computational model are given in Table 1. A linear elastic model was used for the calculation. Due to the nature of the problem to be solved, no significant influence of the plastic behavior of the material was expected.

Table 1. Material properties of the model.

	Bolts 8.8	Other Parts (S355J2G3)
Density	7850 kg·m ⁻³	7830 kg·m ⁻³
Young’s Modulus	2.117 × 10 ⁵ MPa	2.12 × 10 ⁵ MPa
Poisson’s Ratio	0.3	0.29268
Tensile Yield Strength	640 MPa	295 MPa
Tensile Ultimate Strength	800 MPa	450 MPa

The graph (see Figure 10) shows several ways of behavior of the operating load in the bolt. Progress marked as *Real FEM* represents an analysis at the real point of application of the operational force F as in Figure 8. The course of *Theoretical FEM 1* then represents

Assuming a uniform distribution of forces in a symmetrical bolted connection, the following applies:

$$F = F_1 \cdot 4 \quad (9)$$

where:

ΔF_S Force increase in the bolt

F Total operating load

F_1 Operating load to one bolt

C_S Bolt stiffness

C_F Flange stiffness

For the arrangement of Figure 11a, the bolt is lengthened by the operating force, while the compression of the clamped parts is equally reduced. Here, the place of the operational force application is identical to the point of pre-tensioning. Examples of the application of the loads depicted in Figure 11a may include the through bolt connection of a towing eye or crane hook. However, if the point of the operational force application is shifted to the contact surface of the clamped parts (see Figure 11b), a different situation arises. The operating force action increases the extension of the bolt, but the clamped parts are compressed even more. This arrangement changes the stiffness of both the compressing and compressed parts, which affects the change in the form of the diagram used to describe the operating state. This case may occur in a bolted connection of a heat shield, where the bolt is clamping a thermally influenced sheet metal insert. Another example, according to Figure 11b, may occur with some special sealed pressure vessel joints (engine head cover) where the pressure of the medium acts on the area of contact being clamped. In the case of conventional pressure vessels, the problem is the one-sided effect of the operating force at the area of the clamped contact.

In the interval from 0 kN to to 30 kN (see Figure 10) of operating force F it is clear that force increase in the bolt ΔF_S for *Theoretical FEM 1* and *Theoretical* assumption, are much higher compared to “*Real FEM*” behavior. This means that the overall “real” stiffness of components that are even more stressed due to the operating force (e.g., bolt and nut or screwing area) is lower than theoretically predicted, or components that are unloaded due to operating force (e.g., flanges) have a higher value of real stiffness than expected. If the results were to be compared with true reality, the influence of the thread profile in contact would have to be included, but this influence is not the issue in this graphic comparison (the same simplified model was used here for all cases). Nevertheless, Molnar [12] states that by simplifying the “bonded” contact, the stiffness of the tested bolt is increased by 9% (tested on M20 and M24 thread size), which should not interfere with a relevant comparison between the numerical model and the actual state in technical practice.

It should be mentioned that Figure 12 is mainly used for visualization of the stress flow, for this reason the stress legend has been modified. Stresses of magnitude greater than the yield stress of the bolt material (640 MPa) are only negligible in the bolt volume and do not interfere with the linear elastic behavior of the computational model. As shown in Figure 12, the stress (at $F_1 = 8750$ N) spreads to the flange at a smaller angle than the assumed 45° (especially in this case between 34° and 38°). Furthermore, many other publications specify this angle for steels less than 45° , e.g., [13]. This angle can typically be in the range 25° to 33° . The same issue has already been explored in the past. For example, Nassar and Abboud worked together on improving the stiffness model, which is based on a more accurate determination of the effective area of the flange connection (i.e., experimental determination of the strain cone angle) [14]. In this solved case, according to *Theoretical FEM 1* (see Figure 12), it would theoretically mean even less flange stiffness and therefore a greater result of increase in force in the bolt. A similar nature of the stress flow was also found for the *Real FEM* course and thus a different shape of the frustum cone shell is not important for this comparison, as it is not the main cause of the differences in the nature of the curves (see Figure 10).

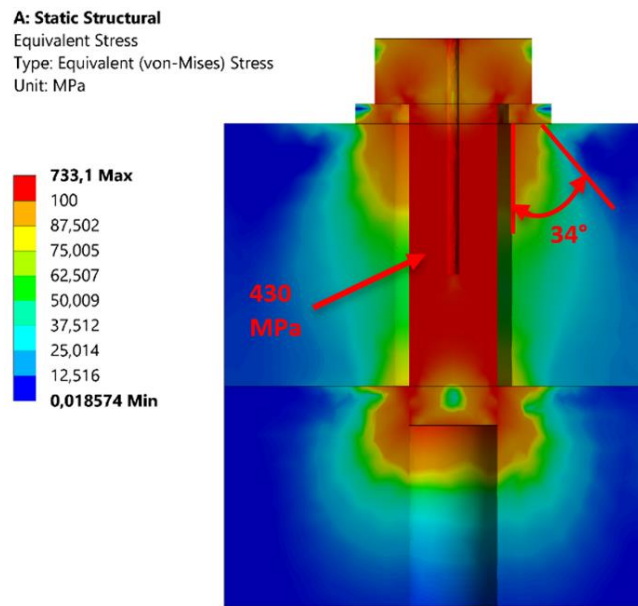


Figure 12. Stress flow by FEM for the course of Theoretical FEM 1.

The assumption named *Theoretical FEM 2* is closer to “real” behavior (see Figure 10), but this is only true for a limited interval (from 0 kN to 25 kN). After that, the curve begins to incline to a larger additional bolt working load. This behavior is probably affected by the characteristics of the total deformation, which is also connected to operating load position against the bolted joint.

The theory further assumes that about one-half of the width of the nut is involved in the stiffness of the bolt. Until the FE analysis was done, it proceeded from the assumption that the first carrier metric thread transfers about 30% of the total load, according to Birger calculation [7] (p. 91), and together with the other two threads they can share more than 60% of the total load. In the distant past, Birger dealt with this issue for metric threads. Hetenyi [15], Jehle [7] (p. 91) and Maduschka [16] dealt with other types of threads (e.g., Whitworth thread). Relatively recently, this problem was also solved using numerical methods such as FEM [17]. The results from experimental measurements and calculations are relatively close together. Due to the simplification of the calculation model, where thread profiles were neglected, and only a cylinder with a defined “bonded” contact was used instead, a screw was used to a depth corresponding to three effective threads.

It has been confirmed that the real behavior of the force increase in the bolt is significantly different compared to the theoretical assumption, despite the fact that at first sight it is a relatively simple, symmetrical, multi-bolted joint (see Figure 8). This fact is already described in [7] (p. 164). At the first stage of loading, there is even a decrease in the bolt force (see detail in Figure 10). This will also be subject to experimental validation. Without the FE analysis, the recalculation of the operating force would be highly implausible.

The obtained dependence showed signs of a power function. With sufficient precision, it was possible to obtain the recalculation equation employing regression (see Figure 10):

$$F = 8984.1 \cdot \Delta F_S^{0.3009} \quad (10)$$

where:

F Total operating load

ΔF_S Increase in the bolt force

This obtained function should be used to convert from the measured bolt working load to the operating load.

4. Preparation of Measuring Bolts

To provide the measurements of the force increases in the bolts, the method of measuring the force using strain gauges on the modified bolts was used. LB11 type strain gauges from the manufacturer HBM [18] were used, which allows installation in an axially drilled hole with a diameter of 2 mm (Figures 13 and 14). For gluing, EP70 adhesive with low viscosity was used.

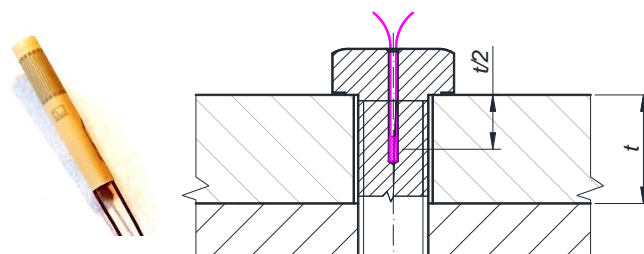


Figure 13. Strain gauge LB11 and its location in the bolt.

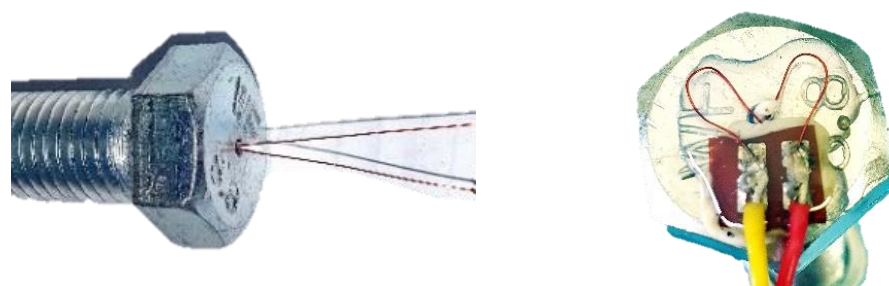


Figure 14. Bolt with installed strain gauge.

Before modification of the bolts, it was necessary to define the correct depth of the strain gauges position, to prevent undesirable spreading of stress flow from the area of the effective thread fitting (e.g., nut) to measurement location. Furthermore, considering the nature of the problem of strain measurement, this is necessary when these items are applied inside the bolt shank without the thread, even if these threads are not “active”. The manufacturers of strain gauges, mentioned here [19], also insist on these conditions. However, these limits only apply to measurements where the force in the bolt is calculated from the strain in gauge fitted inside the shank (i.e., using the so-called “strain gauge constant”), so without any calibration. This issue was discussed by N. Fric and co-authors in [19]. According to their research, it is possible to do this without performing strain-force calibration if the measured bolts have a longer length with a sufficient “strain plateau” for applying strain gauges and if we use adequate coefficients that include the effect of thread along their entire shank (i.e., the difference between the effective and the nominal diameter of the bolt shank with and without thread). Also based on their conclusion, we decided to calibrate each bolt separately (see Figure 15), due to the elimination of the influence of stiffness differences between bolts and thread influence as well.

The conversion constant between the signal from the strain gauge and the axial force applied in the bolt was obtained by measuring on a tensile calibrated testing machine type ZD-40, manufacturer WPM Leipzig. The conversion constant was around 60 kN/(mV/V) and differed by $\pm 8\%$ between the individual bolts. This confirms the appropriateness of separate calibration, recommended in [19], if more reliable measurement is required. The constant determined for a specific bolt and subsequently used in the calculation had a standard deviation of up to 1%, which corresponds to the uncertainty of the tensile testing machine used.

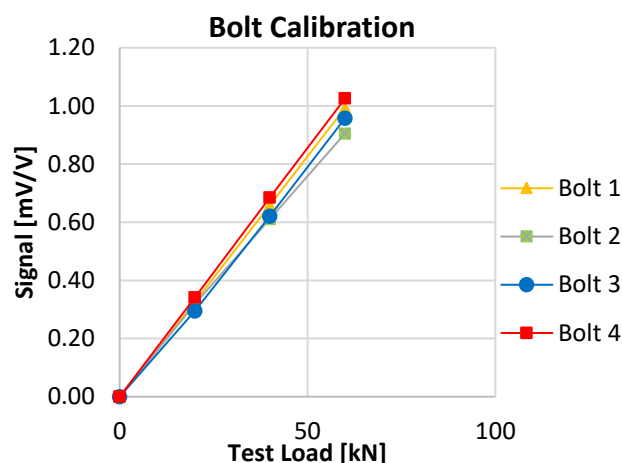


Figure 15. Bolt calibration results.

5. Measurement

Before the measurement itself, it would be necessary to perform correct installation of the bolts on the rolling mill (see Figure 16) and record preliminary data to confirm the correctness of the settings and the polarity of the signal. For technological reasons, the final tightening of the bolts should always be carried out in two steps (see Table 2).

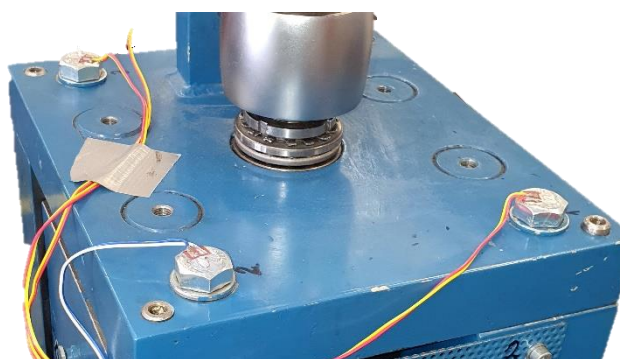


Figure 16. Application of measuring bolts.

Table 2. Steps of bolt tightening (assembly process).

Bolt	Step 1	Step 2	Final Pre-tension
1	39.48 kN	16.98 kN	56.46 kN
2	44.46 kN	19.47 kN	63.93 kN
3	41.29 kN	17.77 kN	59.06 kN
4	40.72 kN	17.05 kN	57.77 kN

Figure 17 depicts the first step of tightening. This measurement is also used to check each bolt pre-tension that assemblers are able to achieve in real conditions when using a torque wrench. Because, as is known e.g., in [20] or in [21], the assembly tightened by the torque control method can vary considerably in the bolt pre-tension achieved, especially in the case of hand tightening. For that reason, many devices have been developed for complex screw fasteners, as for example in [22]. With regard to the fact, that result is the final value of the operating load subsequently determined from the additional force in the bolt, not bolt pre-tension, and the accuracy of the achieved preload can be considered sufficient.

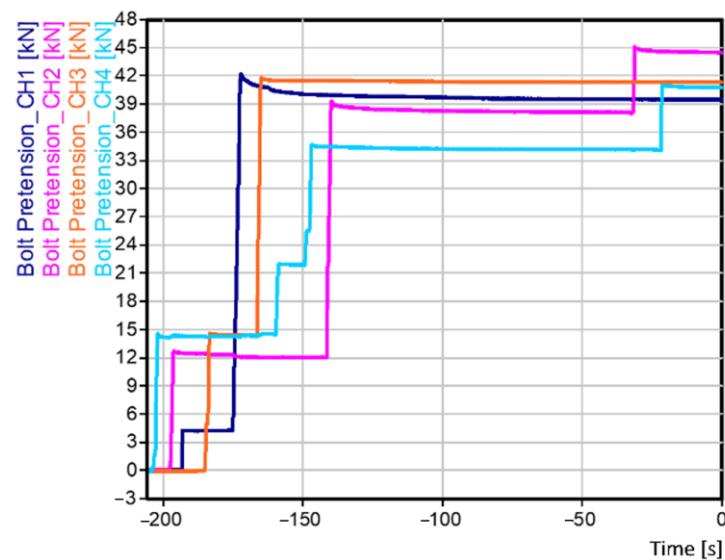


Figure 17. First step of bolt tightening.

This was followed by the measurement of the rolling (operating) forces during the passage of the rolled product. However, the initial measurements already indicated that the theoretical assumptions are not confirmed in the real measurement. All four measured courses should have approximately the same size and polarity, which was only reflected in the signal from bolts 1 and 2 (Channel 1 and Channel 2). The signal from bolt 3 had a significantly larger value and the signal from bolt 4 was significantly smaller and, moreover, negative (see Figure 18).

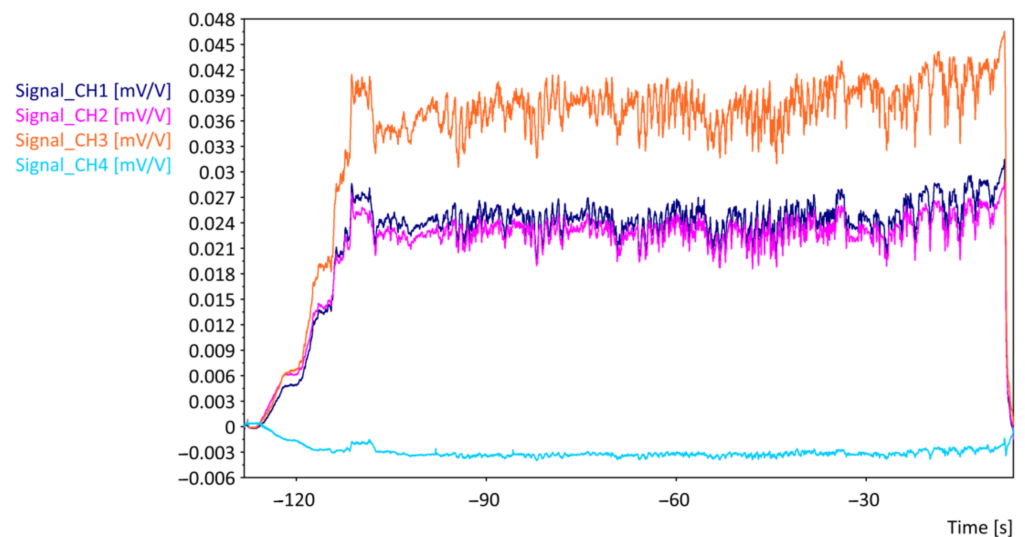


Figure 18. Measurement recording of signal for subsequent recalculation to ΔF_S .

This phenomenon was reflected in all 17 records, which necessitated a re-evaluation of the original conversion curves for the calculation of the rolling force.

An example of a symmetrical component, which in reality may not behave completely symmetrically, can be found e.g., in [23]. Their component was stressed more on one side during the experiment, which also caused the earlier occurrence of a critically stressed bolted joint. However, their numerical simulation no longer included this asymmetry.

The question is what causes similar deviations of apparent symmetry. It can be the eccentricity of the loading device itself, or the deviation in the achieved bolt pre-tension

between the bolts or the imperfect geometry of the clamped parts. There is also another question of how to modify a perfect numerical model to reach a better match with reality.

6. Simulation of the Operating Condition Using FEM

By analyzing the operating conditions and measuring the production tolerances on the measuring equipment, it was found that the parallelism of the contact surfaces between the lid and the body of the rolling mill was not observed during the production of the equipment, which is not significant for the equipment, but for our measurements it is. The actual position of the operating force was also analyzed directly at the measurement location, but without confirmation of the deviation. This condition was also verified by numerical calculation. It has been proven that to achieve the results from Figure 18, the position deviation would have to be significant. The effect of the squareness (flatness) of the bearing surface under the nut to clamp force was previously demonstrated [21]. However, they dealt with force measurement (detection) error in the assembled state or during joint maintenance (after the operation has stopped) in relation to their measurement methodology. In our case, we are dealing with a spatial rupture of symmetry (that is, flatness), which affects the operating force in relation to multiple bolts. A reverse FE analysis was therefore carried out. In other words, such manufacturing deviations of the contact flatness were sought, which would affect the resulting increases in forces in the partial bolts similar to those recorded in the measurements (see Figure 18), where it was first necessary to recalculate the signal values according to the calibration results (see Figure 15). For purpose of reverse analysis, an extensive iterative process was used, where, using the ANSYS software, the lengths of legs L1, L2, L3 and L4 (see Figure 1) were gradually changed, until the desired result was reached (see Figure 19). It was, therefore, necessary to apply controlled asymmetry to the ideally symmetrical model. For this purpose, it was necessary to shorten the length L1 by 0.266 mm, length L2 by 0.49 mm and length L3 by 0.36 mm. The length of the L4 leg remained unchanged. The steps on the horizontal axis of the graph (see Figure 19) only represent the progressive loading of the operating force F .

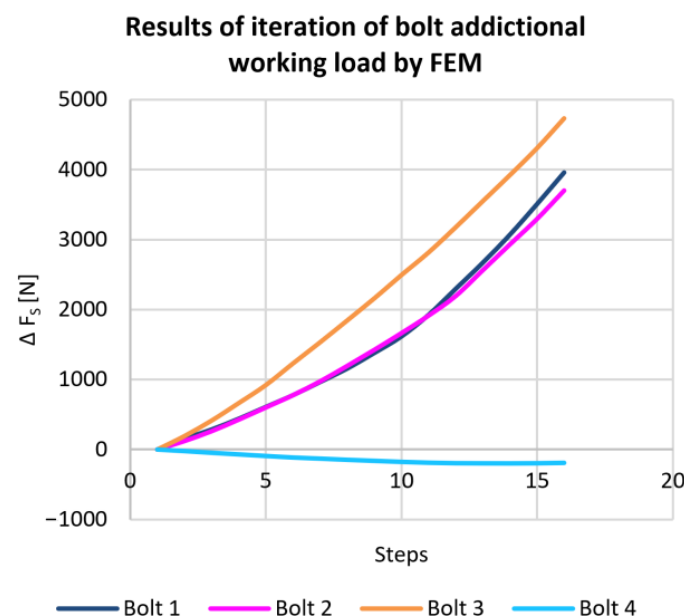


Figure 19. Integration recalculation results obtained with FEM.

The following graph shows the resulting dependence of the operating rolling force F on the additional force in the bolt. Based on these curves, conversion equations were defined (see Figure 20).

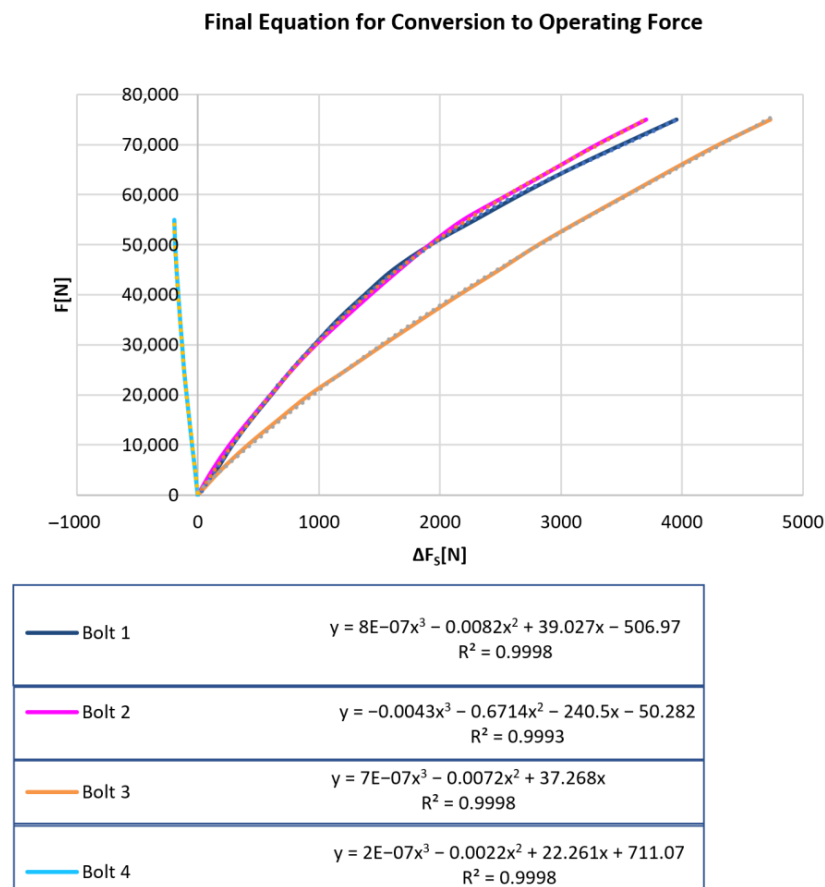


Figure 20. Resulting equations for conversion to the operating load.

For FEM analysis, the values of bolt pre-tension from Table 2 were used. A variant with a preload of 60 kN for each bolt was also verified to show the effect of tightening accuracy. However, this had no significant effect on the character of the curves. Certain differences were visible only in absolute values. For example, the additional operating load to Bolt 1 was then in average 6% lower, Bolt 2 approx. 6.8% higher, Bolt 3 about 2.8% lower and Bolt 4 up to 14.9% lower.

For regressions, it was also possible to use the power function in a limited interval, but in the end, polynomial regression was used, especially with regard to the fact that with the help of the polynomial function, it was possible to achieve a higher reliability value R^2 and the interval of the expected operating force was known in advance. The results of the recalculated values of the operating forces from each bolt are shown in the following graph (Figure 21). The aim was to achieve the most uniform values of the operating force F across the measuring bolts (Bolt1, Bolt2, Bolt3 and Bolt4). The need for greater signal CH4 amplification also caused an increase of visible “signal noise” and slight value differences as well. However, still, the result can be considered satisfactory. For other measured channels (CH1, CH2, CH3), a strong consensus was reached in the resulting value of the operational force, which proves that the equations from the FEM (see Figure 20) work correctly. The marking of the measured channel (see Figure 21) corresponds to the marking of the bolts in Figure 1.

As already mentioned in the introduction of the article, the aim of the measurement was to obtain the value of the operating force F , which could not be measured directly without structural modifications of the whole device. However, these modifications were not allowed. The only option was to measure the bolt pre-tension and then reverse the approach using a FEM. The validity of the methodology and the results obtained (see Figure 21) was verified by practice. In fact, the analyzed rolling mill had experienced

problems in the past from overloading the system. The calculated results of the operating force not only corresponded to the level and type of damage, but also served as a solution to the problem.

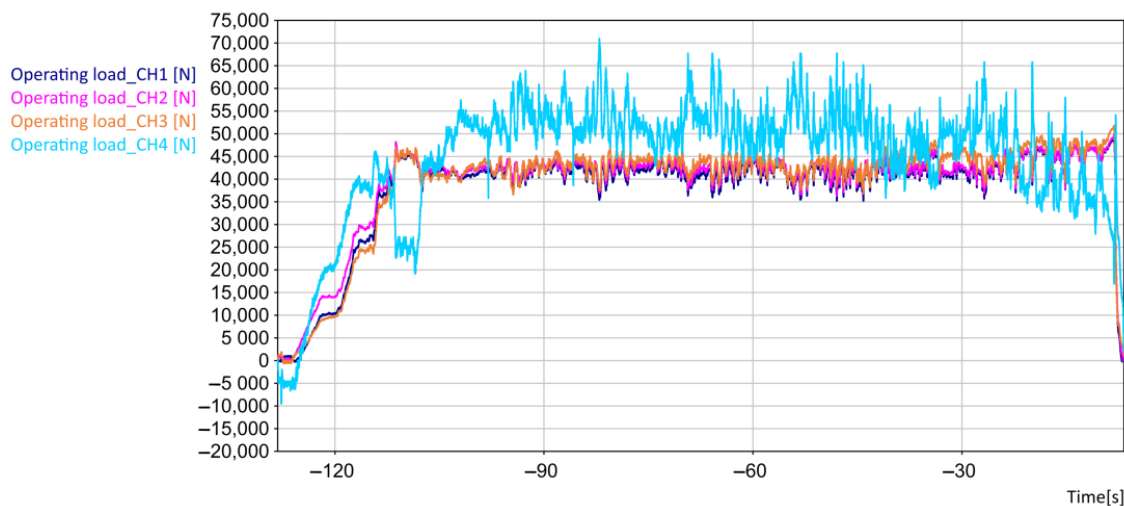


Figure 21. Resulting operating force values.

7. Conclusions

The results of the measurements have shown that for some joints it is very difficult to determine the specific stiffness value of the compressed or compressing parts of the joint during operating conditions. This is mainly due to the complex application of the operational force, which can change its point of action depending on the deformation of the joint parts. This research achieved the following results:

- The influence of asymmetry (deviations from the ideal geometry) of a multiple bolted connection on the working loads of the partial bolts has been proved. Thus, performing an accurate calculation of the operational force increase in the bolt, using the standard calculation procedure specified in Section 2, may not even be possible.
- It has also proved useful to use software based on the FE method. Using the experiment, it was possible to verify that a correctly set FEM calculation can be in strong mutual agreement with reality if any deviations from the ideal model are also included in the calculation model. In other words, FEM software and experiments (e.g., using strain gauges) can complement each other.
- In this particular case, the combination of both approaches made it possible to obtain the value of the otherwise immeasurable magnitude of the operating rolling force F of the rolling device.

The finite element method has thus extended the range of strain gauge measurement. As has been shown, e.g., in [10], sometimes even the experiment itself may not be conclusive due to the fact that additional operating bolt load is not only tensional but a combination of tension and bending and it is not possible to place strain gauges in the ideal position. For that reason, it is also not always advisable to put only one strain gauge per bolt (especially if it is on the outside of the shell of the bolt shank), as for example in [23] (p. 10.). It depends on the type and setting of the experiment, because sometimes there can be a problem with the reproducibility of the measurements.

Of course, there are influences that cannot be completely included in the finite element model. However, if it concerns some effects of geometric deviations of the component or assembly, there is a possibility. It seems that in the case of bolted joints, it is important to consider the prescription and compliance with construction geometric tolerances not only from the point of view of assembling, but also with regard to the operating load (e.g., by maintaining symmetry) of these highly loaded machine parts.

Since the issue of the working force behavior in the bolt also concerns a very important issue of sealed circular flange joints on pressure vessels, the next phase of the research will be aimed at performing similar tests under laboratory conditions.

Author Contributions: Conceptualization, J.Z. and Z.F.; methodology, J.Z. and Z.F.; validation, J.Z., Z.F. and M.T.; formal analysis, J.Z.; investigation, J.S. and J.Z.; resources, J.S.; data curation, J.Z.; writing—original draft preparation, Z.F. and J.Z.; writing—review and editing, J.Z.; visualization, J.Z. and Z.F.; supervision, M.T. All authors have read and agreed to the published version of the manuscript.

Funding: This research received no external funding.

Data Availability Statement: Data are contained within this article. Possible supplementary materials are available on request from the corresponding author.

Conflicts of Interest: The authors declare no conflict of interest.

References

1. Hosoya, N.; Hosokawa, T.; Kajiwara, I.; Hashimura, S.; Huda, F. Evaluation of the Clamping Force of Bolted Joints Using Local Mode Characteristics of a Bolt Head. *J. Nondestruct. Eval.* **2018**, *37*, 75. [CrossRef]
2. Huang, Y.H.; Liu, L.; Yeung, T.W.; Hung, Y.Y. Real-Time Monitoring of Clamping Force of a Bolted Joint by Use of Automatic Digital Image Correlation. *Opt. Laser Technol.* **2009**, *41*, 408–414. [CrossRef]
3. Bolek, A.; Kochman, J. *Machine Parts 5*; SNTL: Praha, Czech Republic, 1989; Volume 1, ISBN 80-03-00046-7.
4. Mynar, V. *Machine Parts—Connecting Parts*; Editorial Centre of VSB-TUO: Ostrava, Czechia, 1975.
5. Tian, Y.; Qian, H.; Cao, Z.; Zhang, D.; Jiang, D.; Lim, J.H.; Luongo, A. Identification of Pre-Tightening Torque Dependent Parameters for Empirical Modeling of Bolted Joints. *Appl. Sci.* **2021**, *11*, 9134. [CrossRef]
6. Zagal, J.; Pavlik, J.; Kunzova, I. Influence of Shape of Pressure Vessel Shell on Bolt Working Load and Tightness. *MM Sci. J.* **2021**, *2021*, 5448–5451. [CrossRef]
7. *Frantisek Pospisil Threaded and Bolted Connections*; SNTL: Praha, Czech Republic, 1968; Volume DT 621.882.
8. Grzejda, R. Impact of Nonlinearity on Bolt Forces in Multi-Bolted Joints: A Case of the Assembly Stage. *Scien-Tia Iran.* **2019**, *26*, 1299–1306. [CrossRef]
9. Grzejda, R. Study of the Distribution of Bolt Forces in a Multi-Bolted System under Operational Normal Loads. In *AIP Conference Proceedings, Bydgoszcz, Poland, 4 March 2019*; American Institute of Physics: College Park, MD, USA, 2019; Volume 2078, p. 020011. [CrossRef]
10. Oman, S.; Nagode, M. Bolted Connection of an End-Plate Cantilever Beam: The Distribution of Operating Force. *Stroj. Vestn./J. Mech. Eng.* **2017**, *63*, 617–627. [CrossRef]
11. Benhaddou, T.; Stéphan, P.; Daidié, A.; Alkatan, F.; Chirol, C.; Tuery, J.-B. Advanced Composite Materials and Processing; Robotics; Information Management. *HAL Open Sci.* **2012**, *3*, 10. [CrossRef]
12. Molnar, L.; Váradi, K.; Liktor, B. Stress Analysis of Bolted Joints Part I. Numerical Dimensioning Method. *Mod. Mech. Eng.* **2014**, *4*, 43267. [CrossRef]
13. Harlalka, A.D.; Slocum, A.H. An Analytical Model for Pitch Moment Stiffness of Bolted Connections and Its Application in Ballscrew Bearing Support Block Selection. *ASME Open J. Eng.* **2022**, *1*, 011027. [CrossRef]
14. Nassar, S.A.; Abboud, A. An Improved Stiffness Model for Bolted Joints. *J. Mech. Des.* **2009**, *131*, 121001. [CrossRef]
15. Hetenyi, M. The Distribution of Stress in Threaded Connections. *Exp. Stress Anal.* **1943**, *1*, 1.
16. Maduschka, L. Beanspruchung von Schraubenverbindungen Und Zweckmäßige Gestaltung Der Gewindeträger. *Forsch. Auf. Dem. Geb. Des. Ing.* **1936**, *7*, 299–305. [CrossRef]
17. Fathalla, A.S.M.; Farid, A.A.; Moezzi, R.; Koloor, S.S.R. A Numerical Study of the Effect of Bolt Thread Geometry on the Load Distribution of Continuous Threads. *J. Eng. Res.* **2021**, *10*, 158–173. [CrossRef]
18. HBM Company. HBM Strain Gauges for Measurements in Screws and Bolts. Available online: https://www.hbm.com/en/7452/cylindric-strain-gauges-for-measurements-in-bolts/?product_type_no=LB11/TB21%20Strain%20Gauges%20for%20Measuring%20in%20Screws%20&%20Bolts (accessed on 2 December 2022).
19. Fric, N.; Pavlovic, M.; Budjevac, D.; Miskovic, Z.; Markovic, Z.; Gluhovic, N. Calibration of the Bolt Pre-tension by Strain Gauges vs. FEA. *Gradjevinski Mater. I Konstr.* **2016**, *59*, 3–15. [CrossRef]
20. Hashimura, S.; Komatsu, K.; Inoue, C.; Nakao, T. A New Tightening Method of Bolt/Nut Assembly to Control the Clamping Force. *J. Adv. Mech. Des. Syst. Manuf.* **2008**, *2*, 896–902. [CrossRef]
21. Hashimura, S.; Sakai, H.; Kubota, K.; Ohmi, N.; Otsu, T.; Komatsu, K. Influence of Configuration Error in Bolted Joints on Detection Error of Clamp Force Detection Method. *Int. J. Autom. Technol.* **2021**, *15*, 396–403. [CrossRef]
22. Kanaval, J.; Cezova, E.; Klima, V.; Stary, F. Testing Equipment for Complex Analysis of Screw Fasteners. In *Proceedings of the 58th International Conference of Machine Design Departments (ICMD), Prague, Czech Republic, 6–8 September 2017*; Herak, D., Ed.; Czech University of Life Sciences Prague: Prague, Czech Republic, 2017; pp. 140–143.

23. Zhang, M.; Yang, M.; Li, P.; Gao, Y. Mechanical Behaviors of a Symmetrical Bolt Fasten Wedge Active Joint for Braced Excavations. *Symmetry* **2020**, *12*, 140. [[CrossRef](#)]
24. Sharos, P.A.; McCarthy, C.T. Novel Finite Element for near Real-Time Design Decisions in Multi-Fastener Composite Bolted Joints under Various Loading Rates. *Compos. Struct.* **2020**, *240*, 112005. [[CrossRef](#)]
25. Belardi, V.G.; Fanelli, P.; Vivio, F. Analysis of Multi-Bolt Composite Joints with a User-Defined Finite Element for the Evaluation of Load Distribution and Secondary Bending. *Compos. B Eng.* **2021**, *227*, 109378. [[CrossRef](#)]

Disclaimer/Publisher's Note: The statements, opinions and data contained in all publications are solely those of the individual author(s) and contributor(s) and not of MDPI and/or the editor(s). MDPI and/or the editor(s) disclaim responsibility for any injury to people or property resulting from any ideas, methods, instructions or products referred to in the content.